DOI 10.1007/s10778-015-0681-y
International Applied Mechanics, Vol. 51, No. 2, March, 2015

STRESSES IN A SPHERICAL SHELL LOADED THROUGH RIGID INCLUSIONS

V. P. Shevchenko and S. V. Zakora

The stress state of a shallow isotropic spherical shell with circular rigid inclusions subject to a force or a moment is determined. The case of two inclusions of unequal radii is analyzed numerically. It is established that the stresses in the shell increase substantially with decrease in the inclusion radius and the distance between the two inclusions

Keywords: shallow isotropic spherical shell, stress state, circular rigid inclusion, bridge between inclusions

Introduction. The analysis of the stress state of shells and plates with various stress concentrators such as holes and inclusions [2–12], concentrated [1] and local [3] loads is still of theoretic and practical interest.

Analytic and numerical solutions for a spherical shell loaded by a force or a moment through a rigid ring were obtained in [3] for a shell with one perfectly rigid inclusion. However, studies of shells and plates with two circular holes or rigid inclusions showed that the stress concentration can be very high if the stress concentrators are close to each other [2, 4–12]. In view of this, we will consider a spherical shell with two circular perfectly rigid inclusions loaded by a force or a moment and will analyze in detail the stress state of a shell with two unequal rigid rings, including the case where they are very close to each other.

1. Problem Formulation. Consider a shallow isotropic spherical shell with m circular perfectly rigid inclusions with centers located on the Ox-axis. The following boundary conditions are defined on the rigid boundaries Γ_q of the inclusions [2]:

$$\varepsilon_{\tau\tau}|_{\Gamma_q} = 0, \quad \kappa_{\tau\tau}|_{\Gamma_q} = 0, \quad \kappa_{\tau\nu}|_{\Gamma_q} = 0, \quad \kappa_{n\tau}|_{\Gamma_q} = 0 \quad (q = \overline{1,m}). \tag{1}$$

Assume that the rigid rings are loaded by transverse forces with resultant component $F_z^{(q)} \neq 0$ or by moments with resultant component $B_y^{(q)} \neq 0$.

The stress state perturbed by the inclusions is determined from the homogeneous governing differential equation for thin spherical isotropic shells proposed in [2]:

$$\nabla^2\nabla^2 U + i\nabla^2 U = 0, \tag{2}$$

where U is an unknown complex function; $\nabla^2 = \dfrac{\partial^2}{\partial\rho^2} + \dfrac{1}{\rho}\dfrac{\partial}{\partial\rho} + \dfrac{1}{\rho^2}\dfrac{\partial^2}{\partial\theta^2}$ is the Laplacian in polar coordinates ρ, θ; $\rho = \dfrac{r}{\sqrt{cR}}$ is a relative dimensionless position vector; $re^{i\theta} = x + iy$, $c = h/\sqrt{12(1-\nu^2)}$; ν is Poisson's ratio; R is the radius of the midsurface of the shell; h is the thickness of the shell; i is imaginary unit.

2. Problem-Solving Method. The solution of the homogeneous differential equation (2) is represented as the sum of cylindrical, polyharmonic, and analytic components:

$$U = U_c + U_p + U_a. \tag{3}$$

Donetsk National University, 21 600-letiya St., Vinnitsa, Ukraine 21021, e-mail: zakora41@yandex.ua. Translated from Prikladnaya Mekhanika, Vol. 51, No. 2, pp. 45–53, March–April 2015. Original article submitted May 24, 2012.

The solutions satisfying the conditions for the symmetry of the stress state about the *Ox*-axis and decreasing in absolute value with distance from Γ_q have the following form [2]:

$$U_{\mathrm{c}}(\rho_q,\theta_q)=\sum_{q=1}^{m}\sum_{n=0}^{\infty}c_{qn}H_n^{(1)}(\sigma\rho_q)\cos n\theta_q, \tag{4}$$

$$U_{\mathrm{p}}(\rho_q,\theta_q)=\sum_{q=1}^{m}\sum_{n=1}^{\infty}a_{qn}\frac{1}{\rho_q^n}\cos n\theta_q, \tag{5}$$

where c_{qn} and a_{qn} are complex unknowns; $H_n^{(1)}(\sigma\rho_q)$ is the Hankel function; $\rho_q=\dfrac{r_q}{\sqrt{cR}}$ is a relative dimensionless position vector in a polar coordinate system $r_q e^{i\theta_q}=x_q+iy_q$ with the origin at the center O_q of the boundary Γ_q; $\sigma=(1+i)/\sqrt{2}$.

The resultant and the principal moment of the external load applied to one of the rigid rings Γ_q are determined as follows [2]:

$$F_x^{(q)}=2\pi EhcR\,\mathrm{Im}(\alpha_1^{(q)}-\alpha_2^{(q)}),$$

$$F_y^{(q)}=2\pi EhcR\,\mathrm{Re}(\alpha_1^{(q)}-\alpha_2^{(q)}), \tag{6}$$

$$B_x^{(q)}=\pi Ehc\,\mathrm{Re}\Big[(\gamma_1^{(q)}-\gamma_2^{(q)})+2icR(1-\nu)(\alpha_1^{(q)}+\alpha_2^{(q)})\Big],$$

$$B_y^{(q)}=\pi Ehc\,\mathrm{Im}\Big[(\gamma_1^{(q)}-\gamma_2^{(q)})-2icR(1-\nu)(\alpha_1^{(q)}+\alpha_2^{(q)})\Big], \tag{7}$$

$$F_z^{(q)}=\pi Ehc\,\mathrm{Im}(\beta_1^{(q)}-\beta_2^{(q)}),$$

$$B_z^{(q)}=\pi EhcR\,\mathrm{Re}(\beta_2^{(q)}-\beta_1^{(q)}). \tag{8}$$

Following [2], it is also necessary to satisfy the uniqueness condition for the complex displacements on the boundaries Γ_q:

$$\alpha_1^{(q)}=-\alpha_2^{(q)},\qquad \beta_1^{(q)}=-\beta_2^{(q)},$$

$$\gamma_1^{(q)}+\gamma_2^{(q)}=-4icR(1+\nu)\overline{\alpha}_1^{(q)}. \tag{9}$$

The complex unknown constants $\alpha_j^{(q)},\beta_j^{(q)},\gamma_j^{(q)}$ $(j=\overline{1,2})$ are determined from the system of equations (6)–(9), given the components of the resultant and principal moment of the external load.

Consider two cases of loading: the rigid rings are loaded by (i) transverse forces, i.e., $F_z^{(q)}\neq 0$, and by (ii) moments $B_y^{(q)}\neq 0$, and $F_x^{(q)}=0, F_y^{(q)}=0, B_x^{(q)}=0, B_z^{(q)}=0$. Then it follows from (6)–(9) that $\alpha_j^{(q)}=0, \overline{\beta_2^{(q)}}=\beta_1^{(q)}, \overline{\gamma_2^{(q)}}=\gamma_1^{(q)}$, and the analytic part U_{a} takes the following form [2]:

$$U_{\mathrm{a}}(r_q,\theta_q)=-\sum_{q=1}^{m}\left[\beta_1^{(q)}(1+\ln r_q)+\gamma_1^{(q)}\frac{1}{r_q}\cos\theta_q\right]. \tag{10}$$

To separate variables in the function U in the qth coordinate system, we will use an approached [2] that is based on Graf's theorem for cylindrical functions in (4) and involves the expansion of each term of the power part (5) and the analytical part (10) of the solution into a Laurent series. In the case of two rigid inclusions ($m=2$), we have

$$U_{\mathrm{c}}(\rho_q,\theta_q)=\sum_{q=1}^{2}\sum_{n=0}^{\infty}$$

$$\times\left\{J_n(\sigma\rho_{0q})e_n\sum_{p=0}^{\infty}e_{np}c_{3-q\,p}\left[H_{n-p}^{(1)}(\sigma l)+(-1)^p H_{n+p}^{(1)}(\sigma l)\right]+c_{qn}H_n(\sigma\rho_{0q})\right\}\cos n\theta_q, \tag{11}$$

$$U_{\mathrm{p}}(\rho_q,\theta_q)=\sum_{q=1}^{2}\left[\sum_{n=0}^{\infty}\sum_{p=2}^{\infty}\frac{(-1)^n(p+n-1)!\rho_{0q}^n}{(p-1)!n!l_1^{p+n}}a_{3-q\,p}\cos n\theta_q+\sum_{n=2}^{\infty}a_{qn}\frac{1}{\rho_{0q}^n}\cos n\theta_q\right], \tag{12}$$

$$U_{\mathrm{a}}(\rho_q,\theta_q)=-\sum_{q=1}^{2}\left\{\beta_1\left[2+\ln\rho_{0q}+\ln l+\sum_{n=1}^{\infty}\frac{(-1)^{n+1}}{n\cdot l_1^n}\rho_{0q}^n\cos n\theta_q\right]\right.$$

$$\left.+\gamma_1\left[\frac{1}{\rho_{0q}}\cos\theta_q-\sum_{n=0}^{\infty}\frac{(-1)^n}{l_1^{n+1}}\rho_{0q}^n\cos n\theta_q\right]\right\}, \tag{13}$$

where $J_n(\sigma\rho_{0q})$ is the Bessel function of the first kind; $\rho_{0q}=\dfrac{r_{0q}}{\sqrt{cR}}$ is the dimensionless radius of the qth inclusion; $l=L/\sqrt{cR}$, L is the distance between the centers of the circles O_1O_2 (Fig. 1);

$$l_1=l(-1)^q,\qquad e_n=\begin{cases}1/2, & n=0,\\ 1, & n\neq 0,\end{cases}\qquad e_{np}=\begin{cases}1, & q=1,\\ (-1)^{n+p}, & q=2.\end{cases}$$

The boundary strains (1) are expressed as

$$\varepsilon_{\tau\tau}=T_\theta-\nu T_r,\qquad \kappa_{\tau\tau}=\frac{6}{h}(G_\theta-\nu G_r),$$

$$\kappa_{\tau\nu}=\frac{6(1+\nu)}{h}H_{r\theta},\qquad \kappa_{n\tau}=\frac{d(T_r+T_\theta)}{dr}-\frac{(1+\nu)}{r}\frac{dS_{r\theta}}{d\theta}. \tag{14}$$

The forces and moments corresponding to solutions (11)–(13) are expressed as follows [2, 3]:

$$T_r=-\frac{1}{\rho}\operatorname{Im}\left(\frac{\partial U}{\partial\rho}+\frac{1}{\rho}\frac{\partial^2U}{\partial\theta^2}\right),\qquad S_{r\theta}=\operatorname{Im}\frac{\partial}{\partial\rho}\left(\frac{1}{\rho}\frac{\partial U}{\partial\theta}\right),$$

$$H_{r\theta}=-(1-\nu)c\operatorname{Re}\frac{\partial}{\partial\rho}\left(\frac{1}{\rho}\frac{\partial U}{\partial\theta}\right),\qquad T_\theta=-\operatorname{Im}\frac{\partial^2U}{\partial\rho^2},$$

$$G_r=-c\operatorname{Re}\left(\frac{\partial^2U}{\partial\rho^2}+\frac{\nu}{\rho}\frac{\partial U}{\partial\rho}+\frac{\nu}{\rho^2}\frac{\partial^2U}{\partial\theta^2}\right),\qquad G_\theta=-(1+\nu)c\operatorname{Re}\nabla^2U-G_r. \tag{15}$$

Let the rigid rings be loaded by equal transverse forces, i.e., $F_z^{(q)}=F_z$, and by equal moments $B_y^{(q)}=B_y(-1)^{q+1}$. When $F_z=\pi Ehc$ and the other components are equal to zero, the system of equations (6)–(9) yields

$$\alpha_1^{(q)}=0,\quad \alpha_2^{(q)}=0,\quad \beta_1^{(q)}=\frac{i}{2},\quad \beta_2^{(q)}=-\frac{i}{2},\quad \gamma_1^{(q)}=0,\quad \gamma_2^{(q)}=0, \tag{16}$$

when $B_y=\pi Ehc\sqrt{cR}$, we have

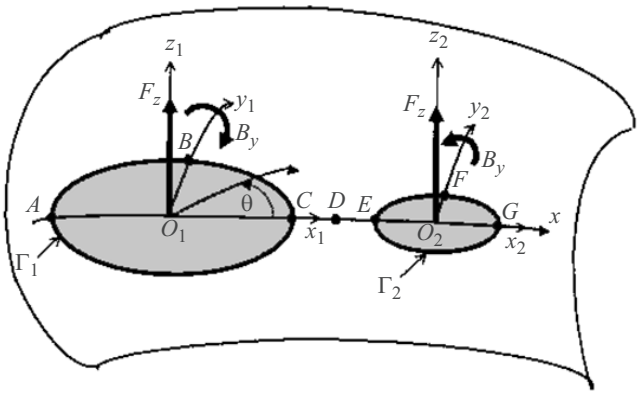

Fig. 1

$$\alpha_1^{(q)} = 0,\ \alpha_2^{(q)} = 0,\quad \beta_1^{(q)} = 0,\quad \beta_2^{(q)} = 0,\quad \gamma_1^{(q)} = (-1)^{q+1}\,\frac{i}{2}\sqrt{cR},\quad \gamma_2^{(q)} = (-1)^{q}\,\frac{i}{2}\sqrt{cR}. \tag{17}$$

Substituting the forces and moments (15) with (11)–(13) into the boundary conditions (1), (14) and equating the coefficient of like harmonics, we obtain an infinite system of linear algebraic equations for the real and imaginary parts of the unknowns a_{qn} and c_{qn}. Since the complex unknown constants $\alpha_j^{(q)}, \beta_j^{(q)}, \gamma_j^{(q)}$ $(j = \overline{1,2})$ are given by (16), (17), this also defines the right-hand sides of the system.

For the boundary strains (14), the coefficients of the unknown constants are related by

$$\rho\kappa_{\tau\tau}^0 \equiv -\sqrt{3(1-\nu^2)}\,\kappa_{n\tau}^0,\qquad \kappa_{\tau\nu}^0 \equiv 0 \tag{18}$$

for the zeroth harmonic and

$$\kappa_{\tau\tau}^1 \equiv -\kappa_{\tau\nu}^1,\qquad \rho^2\kappa_{\tau\tau}^1 \equiv \sqrt{3(1-\nu^2)}\,(\varepsilon_{\tau\tau}^1 - \rho\kappa_{n\tau}^1) \tag{19}$$

for the first harmonic.

In deriving the system, we omit the equations dependent through identities (18) and (19). For example, we keep $\varepsilon_{\tau\tau}^0|_{\Gamma_1} = 0$, $\kappa_{\tau\tau}^0|_{\Gamma_1} = 0$ for the zeroth harmonic and $\varepsilon_{\tau\tau}^1|_{\Gamma_1} = 0$, $\kappa_{n\tau}^1|_{\Gamma_1} = 0$ and $\kappa_{\tau\tau}^1|_{\Gamma_1} = 0$, or $\kappa_{\tau\nu}^1|_{\Gamma_1} = 0$ for the first harmonic.

The resulting system is solved with the reduction method. Substituting c_{qn} and a_{qn} found by solving the system into formulas (11)–(13) and (3), we find the function U. Next, we use formulas (15) to determine the forces and moments at given points, which are transformed by well-known formulas [2] upon passage to the directions $\vec{\sigma}$ and $\vec{\tau}$. As a result, we obtain the concentration factors for membrane and bending stresses:

$$k_\theta^{\mathrm{T}} = T_\theta / d,\quad k_r^{\mathrm{T}} = T_r / d,\quad k_\theta^{\mathrm{B}} = 6G_\theta / dh,\quad k_r^{\mathrm{B}} = 6G_r / dh,$$

$$\tau_{r\theta}^{\mathrm{T}} = S_{r\theta} / d,\quad \tau_{r\theta}^{\mathrm{B}} = 6H_{r\theta} / dh. \tag{20}$$

They are then used to calculate the relative equivalent stresses using the energy theory of strength [2]:

$$k_\theta = k_\theta^{\mathrm{T}} \pm k_\theta^{\mathrm{B}},\quad k_r = k_r^{\mathrm{T}} \pm k_r^{\mathrm{B}},$$

$$k_{r\theta} = \tau_{r\theta}^{\mathrm{T}} \pm \tau_{r\theta}^{\mathrm{B}},\quad k_{\mathrm{eq}} = \sqrt{k_r^2 + k_\theta^2 - k_r k_\theta + 3k_{r\theta}^2}.$$

The signs "+" and "–" correspond to the relative equivalent stresses on the outside ($k_{\mathrm{eq}}^{\mathrm{Ext}}$) and inside ($k_{\mathrm{eq}}^{\mathrm{Int}}$) surfaces of the shell. In the tables and figures below, the concentration factors are scaled up (10:1); therefore, $d = 0.1Eh$ in formulas (20).

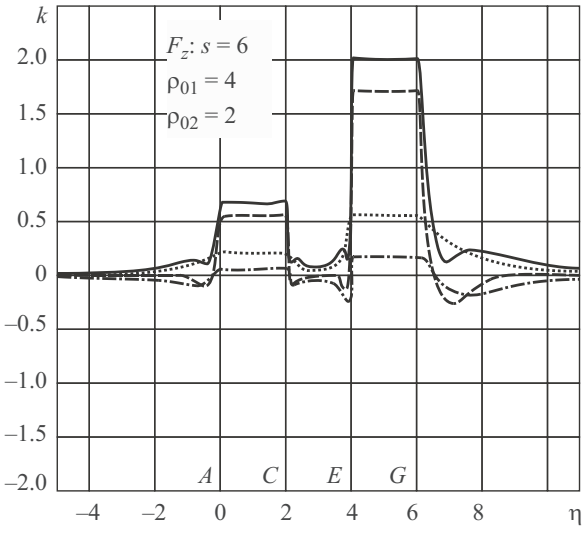

Fig. 2

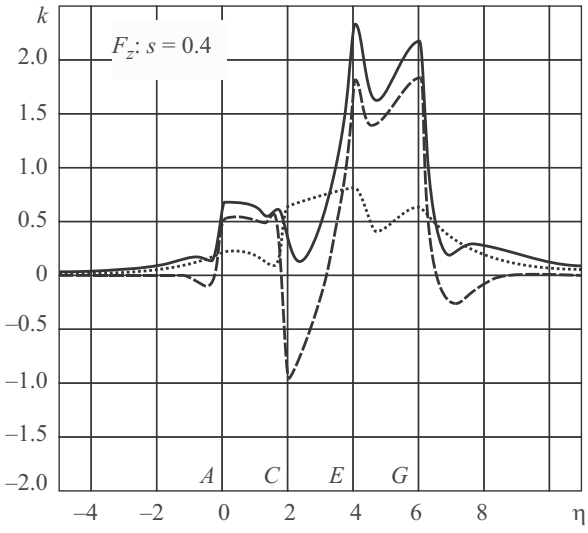

Fig. 3

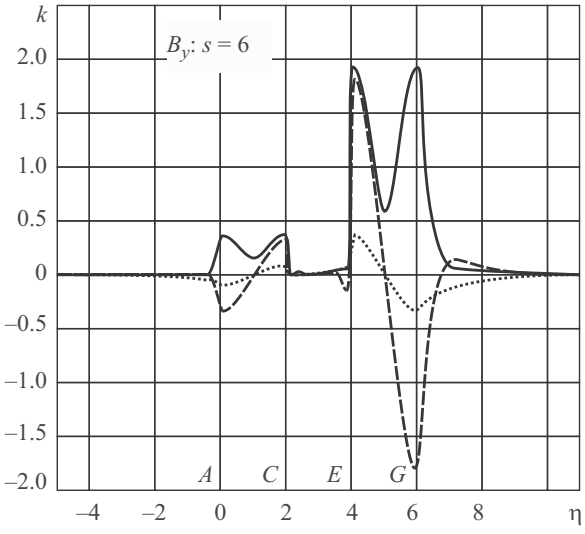

Fig. 4

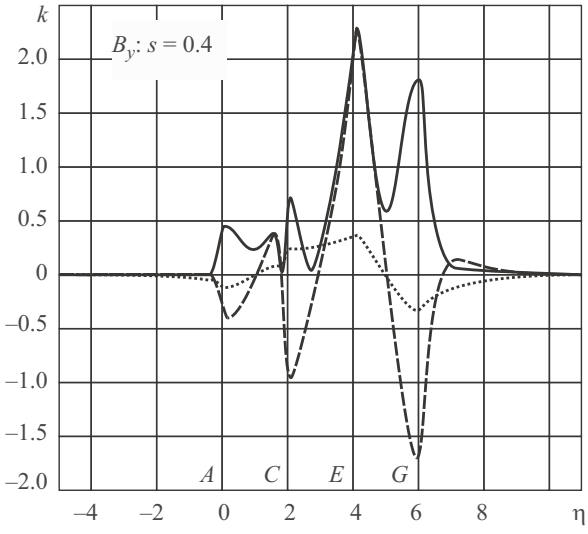

Fig. 5

3. Analysis of the Numerical Results. The numerical analysis has been performed for an isotropic spherical shell (Poisson's ratio $\nu = 0.3$) with two rigid rings of radii $\rho_{01} = 4$ and $\rho_{02} = 2$ for different relative widths s of the bridge between the rings. Here ρ_{0q} are the radii of the inclusions; $s = S / r_{01}$, where S is the width of the bridge between the inclusions (CE in Fig. 1).

In Figs. 2–5, the parameter η laid off along the abscissa axis takes the following values: (i) $\eta = 4q - 4 + \dfrac{2\theta_q^*}{\pi}$, $4(q-1) \le \eta \le 4q-2$, describes half the boundary Γ_q of the inclusion, i.e., if there is symmetry about the Ox-axis, we have $0 \le \theta_q^* \le \pi$, where $\theta_q^* = \pi - \theta_q$ (Fig. 1); (ii) $\eta = 2\left(1 + \dfrac{x_1 - r_{01}}{S}\right)$, $2 \le \eta \le 4$, describes the bridge s, i.e., $r_{01} \le x_1 \le r_{01} + S$; (iii) $\eta = 4q - 3 + x_q / r_{0q}$ describes the distance from the boundary Γ_q along the Ox_q-axis to $5r_{0q}$, i.e., $-5 \le x_1 \le 0$ or $6 \le x_2 \le 11$.

The vertical axis indicates the following relative stresses: equivalent stress on the outside surface $k_{\text{eq}}^{\text{Ext}}$ (solid line), tangential stress k_r^{T} (dotted line), tangential stress k_θ^{T} (dash-and-dot line), and bending stress k_r^{B} (dashed line).

TABLE 1

Case F_z	Points			
	k_r, k_θ, k_{eq}	$\rho_{01} = 4$, from point A to point C, $0 \le \theta_1^* \le \pi$	$s = 7.5$, point D, $s/2$	$\rho_{02} = 2$, from point E to point G, $0 \le \theta_2^* \le \pi$
a	k_r^T	0.203	0.003	0.553
	k_θ^T	0.061	–0.003	0.166
	k_r^B	0.556	0.000	1.700
	k_θ^B	0.167	0.000	0.510
	k_{eq}^{Ext}	0.675	0.004	2.002
	k_{eq}^{Int}	0.314	0.004	1.019

TABLE 2

Case F_z	k_r, k_θ, k_{eq}	$\rho_{01} = 4$			$s = 0.2$	$\rho_{02} = 2$		
		Point A, $\theta_1^* = 0$	Point B, $\theta_1^* = \pi/2$	Point C, $\theta_1^* = \pi$	Point D, $s/2$	Point E, $\theta_2^* = 0$	Point F, $\theta_2^* = \pi/2$	Point G, $\theta_2^* = \pi$
b	k_r^T	0.198	0.208	0.851	0.904	0.926	0.391	0.649
	k_θ^T	0.059	0.062	0.255	0.163	0.278	0.117	0.195
	k_r^B	0.438	0.569	–1.789	–0.101	2.039	1.365	1.956
	k_θ^B	0.131	0.171	–0.537	0.003	0.612	0.409	0.587
	k_{eq}^{Ext}	0.565	0.733	0.834	0.734	2.636	1.564	2.316
	k_{eq}^{Int}	0.214	0.404	2.347	0.935	0.989	0.870	1.161

Figures 2 and 3 show the distribution of stresses and Tables 1 and 2 summarize their values for F_z and for $s = 6$ (Fig. 2), $s = 0.4$ (Fig. 3), for $s = 7.5$ (Table 1) and $s = 0.2$ (Table 2). Similar results for B_y are presented in Figs. 4 and 5 and in Table 3.

The figures and tables indicate that the stress concentration on and near the boundary of the smaller ring is higher than on the larger ring. For example, the maximum stresses k_{eq}^{Ext} and k_{eq}^{Int} on the boundary Γ_2 of radius $\rho_{02} = 2$ are higher than on the boundary Γ_1 of radius $\rho_{01} = 4$ by a factor of 3 for F_z (Fig. 2 and Table 1) and by a factor of 5 to 6 for B_y (Fig. 4 and Table 3*a*). The contribution of the bending stresses k_r^B is the greatest. As the radius of the rigid inclusion is decreased, the zone of decrease in the stress concentration becomes larger.

TABLE 3

Case	k_r, k_θ, k_{eq}	Point A, $\theta_1^* = 0$	Point B, $\theta_1^* = \pi / 2$	Point C, $\theta_1^* = \pi$	Point D, $s / 2$	Point E, $\theta_2^* = 0$	Point F, $\theta_2^* = \pi / 2$	Point G, $\theta_2^* = \pi$
		$\rho_{01} = 4$			$s = 7.5$	$\rho_{02} = 2$		
a	k_r^T	–0.087	0.000	0.087	0.000	0.342	0.000	–0.342
	k_θ^T	–0.026	0.000	0.026	0.000	0.102	0.000	–0.102
	k_r^B	–0.325	0.000	0.325	0.000	1.820	0.000	–1.820
	k_θ^B	–0.098	0.000	0.098	0.000	0.546	0.000	–0.546
	k_{eq}^{Ext}	0.367	0.151	0.367	0.000	1.922	0.592	1.922
	k_{eq}^{Int}	0.212	0.151	0.212	0.000	1.314	0.592	1.314
b	k_r, k_θ	$\rho_{01} = 4$			$s = 0.2$	$\rho_{02} = 2$		
	k_r^T	–0.122	0.042	0.318	0.335	0.370	–0.078	–0.300
	k_θ^T	–0.037	0.013	0.095	0.099	0.111	–0.023	–0.090
	k_r^B	–0.482	0.104	–1.364	0.477	2.712	–0.177	–1.589
	k_θ^B	–0.145	0.031	–0.409	0.211	0.814	–0.053	–0.477
	k_{eq}^{Ext}	0.537	0.294	0.930	0.709	2.739	0.573	1.680
	k_{eq}^{Int}	0.320	0.269	1.496	0.130	2.081	0.533	1.146

Figures 3 and 5 and Tables 2 and 3*b* show that as the bridge width s is decreased, the relative equivalent stresses near and on the bridge increase and the zone of decrease in the stresses with distance from the boundaries along the $-Ox_1$- and Ox_2-axes becomes larger.

Reliability of the Results. 1. We tested the accuracy of satisfying the boundary conditions through the direct calculation of the forces and moments on the boundaries using series (4), (5), (10), i.e., not using Graf's theorem and Laurent series. To this end, we used Maple software. The accuracy of computation can be varied by assigning a value to the system variable Digits and setting the number n of harmonics in (9) and (10). For example, the absolute error of satisfying the boundary conditions did not exceed 10–47 for $n = 30$ and Digits = 50 in the cases represented in Tables 1 and 3*a* and 10^{-4} in the cases represented in Tables 2 and 3*b* (the maximum stresses being less than 3).

2. For comparison to a spherical shell with one rigid inclusion, we calculated the case where the rigid inclusions do not interact, i.e., $s = 7.5$. The results are in good agreement with those obtained in [3].

3. It is also observed that as the radius of the rigid inclusion is decreased, the stress state qualitatively tends to the case of a concentrated force addressed in [1] in all cases (load distributed over the ring).

4. We also tested the accuracy of satisfying the differential equations (1) by the function U with coefficients determined after the solution of the system. The absolute error does not exceed 10^{-46} for Digits = 50.

5. After solving the system, the components of the resultant and principal moment have been evaluated as integrals according to [2] (for example: $B_z = \rho^2 \int_0^{2\pi} S_{r\theta} d\theta$, etc.). The calculated components are in good agreement with the given components. The absolute error does not exceed 10^{-8} for Digits = 10 (the maximum value being less than 20π).

Conclusions. We have presented a method for and performed a numerical analysis of the stress state of a spherical shell with two circular rigid inclusions loaded by transverse forces or moments. It has been established that with decrease in the radius of the inclusion, the relative equivalent stresses on its boundary increase severalfold (by a factor of 3 to 6 in the above examples). The radial bending stresses make the greatest contribution. As the radius of the rigid inclusion is decreased, the zone of decrease in the stress concentration becomes larger.

The results together with the Maple routine developed can be used in engineering to determine the stresses and the zone of their decay in a spherical shell loaded through rigid rings.

REFERENCES

1. P. M. Velichko and V. P. Shevchenko, "The action of concentrated forces and moments on a shell of positive curvature," *Izv. AN SSSR*, *Mekh. Tverd. Tela*, No. 2, 147–151 (1969).
2. A. N. Guz, I. S. Chernyshenko, Val. N. Chekhov, Vik. N. Chekhov, and K. I. Shnerenko, *Theory of Thin Shells Weakened by Holes*, Vol. 1 of the five-volume series *Methods of Shell Design* [in Russian], Naukova Dumka, Kyiv (1980).
3. *Handbook of Strength*, *Stability*, *and Vibrations* [in Russian], Ch. 24, Vol. 3, Mashinostroenie, Moscow (1968).
4. Y. Y. Deryugin and G. V. Lasko, "Field of stresses in an isotropic plane with circular inclusion under tensile stress," *Engineering*, **4**, No. 9, 583–589 (2012).
5. Kh. Fuad, R. A. Siregar, Ch. Rangkuti, B. Ariwahjoedi, and M. Firdaus, "Stress concentration factors of various adjacent holes configurations in a spherical pressure vessel," in: *Proc. 5th Australasian Congr. on Appl. Mech*, ACAM-2007, Brisbane, Australia, December 10–12 (2007), pp. 68–73.
6. F. Li, Y. He, C. Fan, H. Li, and H. Zhang, "Investigation on three-dimensional stress concentration of LY12-CZ plate with two equal circular holes under tension," *Mater. Sci. Eng.*, **A**, 483–484, No. 1–2, 474–476 (2008).
7. D. V. Kubair and B. Bhanu-Chandar, "Stress concentration factor due to a circular hole in functionally graded panels under uniaxial tension," *Int. J. Mech. Sci.*, **50**, No. 4, 732–742 (2008).
8. V. A. Maximuk, E. A. Storozhuk, and I. S. Chernyshenko, "Stress state of flexible composite shells with reinforced holes," *Int. Appl. Mech.*, **50**, No. 5, 558–565 (2014).
9. V. A. Maximuk, E. A. Storozhuk, and I. S. Chernyshenko, "Nonlinear deformation of thin isotropic and orthotropic shells of revolution with reinforced holes and rigid inclusions," *Int. Appl. Mech.*, **49**, No. 6, 685–692 (2013).
10. V. A. Maximuk, E. A. Storozhuk, and I. S. Chernyshenko, "Variational finite-difference methods in linear and nonlinear problems of the deformation of metallic and composite shells," *Int. Appl. Mech.*, **48**, No. 6, 613–687 (2012).
11. M. Miyagawa, T. Suzuki, and J. Shimura, "Analysis of in-plane problems with singular disturbances for an isotropic elastic medium with two circular holes or rigid inclusions," *J. Envir. Eng.*, **6**, No. 4, 778–791 (2011).
12. N. Yahnioglu and Y. U. Babuscu, "Stress concentration in two neighboring circular holes in a composite plate," *An. Univ. Oradea*, *Fasc. Mat.*, **13**, 261–272 (2006).